

# Serial in Vivo Imaging Using a Fluorescence Probe Allows Identification of Tumor Early Response to Cetuximab Immunotherapy

Teng Ma,<sup>†,‡,§</sup> Hao Liu,<sup>†,‡,§</sup> Xianlei Sun,<sup>†,‡</sup> Liquan Gao,<sup>†,‡</sup> Jiyun Shi,<sup>†,§</sup> Huiyun Zhao,<sup>†,||</sup> Bing Jia,<sup>†,‡</sup> Fan Wang,<sup>\*,†,‡,§</sup> and Zhaofei Liu<sup>\*,†,‡</sup>

<sup>†</sup>Medical Isotopes Research Center, Peking University, Beijing 100191, China

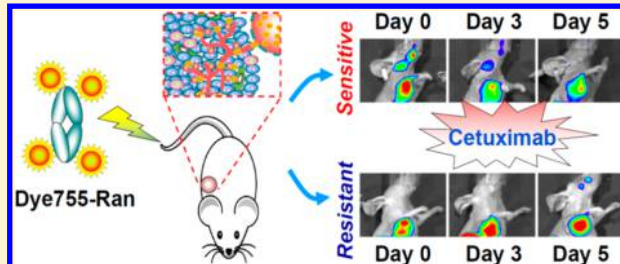
<sup>‡</sup>Department of Radiation Medicine, School of Basic Medical Sciences, Peking University, Beijing 100191, China

<sup>§</sup>Interdisciplinary Laboratory, Institute of Biophysics, Chinese Academy of Sciences, Beijing 100101, China

<sup>||</sup>Medical and Healthy Analytical Center, School of Basic Medical Sciences, Peking University, Beijing 100191, China

## Supporting Information

**ABSTRACT:** Cetuximab is an antiepidermal growth factor receptor (EGFR) monoclonal antibody that has received the approval of the Food and Drug Administration (FDA) for cancer treatment. However, most clinical studies indicate that cetuximab can only elicit positive effects on a subset of cancer patients. In this study, we investigated whether near-infrared fluorescence (NIRF) imaging of tumor vascular endothelial growth factor (VEGF) expression could be a biomarker for tumor early response to cetuximab therapy in preclinical wild-type and mutant tumor models of the KRAS gene. The treatment efficacy of cetuximab was determined in both HT-29 (wild-type *KRAS*) and HTC-116 (mutant *KRAS*) human colon cancer models. A VEGF-specific optical imaging probe (Dye755-Ran) was synthesized by conjugating ranibizumab (an anti-VEGF antibody Fab fragment) with a NIRF dye. Serial optical scans with Dye755-Ran were performed in HT-29 and HTC-116 xenograft models. By using longitudinal NIRF imaging, we were able to detect early tumor response on day 3 and day 5 after initiation of cetuximab treatment in the cetuximab-responsive HT-29 tumor model. Enzyme-linked immunosorbent assay (ELISA) confirmed that cetuximab treatment inhibited human VEGF expression in the *KRAS* wild-type HT-29 tumor but not in the *KRAS* mutant HCT-116 tumor. We have demonstrated that the antitumor effect of cetuximab can be noninvasively monitored by serial fluorescence imaging using Dye755-Ran. VEGF expression detected by optical imaging could serve as a sensitive biomarker for tumor early response to drugs that directly or indirectly act on VEGF.



**KEYWORDS:** molecular imaging, angiogenesis, epidermal growth factor receptor, tumor response, treatment monitoring

## ■ INTRODUCTION

The epidermal growth factor receptor (EGFR) is a member of the HER family, which consists of four members: EGFR (ErbB1/HER1), HER2/neu (ErbB2), HER3 (ErbB3), and HER4 (ErbB4). EGFR is crucial in the development and progression of human carcinomas, and its overexpression is usually associated with poor prognosis.<sup>1</sup> Blockade of the EGFR signaling using either monoclonal antibody (mAb, e.g., cetuximab, and panitumumab) or small-molecule tyrosine kinase inhibitor (TKI, e.g., gefitinib, erlotinib, and lapatinib) has been found to be a promising approach for cancer therapy.<sup>2</sup> Cetuximab (Erbitux) is a chimeric anti-EGFR mAb that has been approved by the Food and Drug Administration (FDA) for the treatment of metastatic colorectal cancer (mCRC) and head and neck cancer. Although promising, cetuximab can only elicit positive effects on a subset of cancer patients. In addition, most patients who received cetuximab manifest either intrinsic resistance or acquired resistance after initially demonstrating

positive results.<sup>3</sup> The expression level of EGFR is not correlated with clinical response to cetuximab.<sup>4,5</sup> Thus, EGFR expression is not a predictor of tumor response.<sup>6,7</sup> These observations, together with the side effects and high costs of mAb-based immunotherapy, have necessitated investigations on the early predictive biomarkers of tumor response to cetuximab therapy.

In the past decade, strong clinical evidence has demonstrated that the efficacy of cetuximab is limited to mCRC patients whose tumor carries a wild-type *KRAS* gene,<sup>8,9</sup> which indicates that *KRAS* status is a predictive factor.<sup>10</sup> Considering these findings, the FDA has altered the usage labels on cetuximab and panitumumab and affirmed that both drugs are not recommended for the treatment of colorectal cancer with

**Received:** April 23, 2014

**Revised:** September 24, 2014

**Accepted:** November 14, 2014

**Published:** November 14, 2014



KRAS mutations.<sup>11</sup> However, biopsied tumor samples are predominantly used for KRAS gene mutation analysis.<sup>10,12</sup> Tumor biopsy is an invasive procedure that cannot be frequently repeated. Analysis of biopsied tumor samples may not provide complete information on the tumor because of tumor heterogeneity and gene expression discordance in primary and metastatic lesions.<sup>13</sup> Moreover, identification of predictive biomarkers, such as KRAS gene, before the start of actual treatment only predicts high probabilities of tumor response to therapy. Some patients with positive predictive biomarkers will not certainly respond.<sup>14</sup> A previous meta-analysis indicated that approximately 50% of patients with wild-type KRAS failed to respond to cetuximab, but that 9% of cetuximab responders were KRAS mutant patients.<sup>15,16</sup> Hence, new approaches that can accurately assess therapeutic response at the earliest stage in a noninvasive and dynamic manner through whole-body imaging are needed.

Molecular imaging techniques, such as positron emission tomography (PET), single-photon-emission computed tomography (SPECT), and optical imaging have recently received increasing attention for early tumor detection, patient stratification, and image-guided cancer treatment. Molecular imaging can noninvasively detect molecular changes during cancer treatment, which occur earlier than anatomical changes, such as decrease in tumor volume. Compared with PET and SPECT, optical imaging techniques, such as near-infrared fluorescence (NIRF) imaging, are limited in the depth of tissue penetration and are not routine clinical modalities. However, NIRF does not require the use of radioactive materials. Moreover, the imaging system and scan process of NIRF are low cost and fast, respectively. The optical imaging probes for NIRF are usually less expensive and much easier to generate than radiotracers. Optical imaging also facilitates multicolor imaging using fluorophores with different emission wavelengths.<sup>17</sup>

Angiogenesis is crucial for tumor growth, invasion, and metastasis formation. A predominant regulator of tumor angiogenesis is the vascular endothelial growth factor (VEGF)/VEGF receptor (VEGFR) pathway, which induces the proliferation and migration of endothelial cells.<sup>18</sup> Inhibition of VEGF/VEGFR signaling using the VEGF-specific antibody bevacizumab or VEGFR-targeted TKIs is clinically proven to have antitumor efficacy.<sup>19</sup> VEGF shares downstream signaling components with EGFR,<sup>20,21</sup> and EGFR inhibition agents (e.g., antibodies and TKIs) can induce down-regulation of VEGF and other angiogenic growth factors, such as interleukin 8 (IL-8) and basic fibroblast growth factor (FGF).<sup>3,22</sup> The antitumor effect of cetuximab is considered to be, at least partly, mediated by the inhibition of angiogenesis by interrupting the VEGF signaling pathway.<sup>21,23</sup> On the basis of these findings, we hypothesized that VEGF expression detected by noninvasive imaging might be an early biomarker for cetuximab cancer therapy.

Recently, we have demonstrated that optical imaging using near-infrared fluorophore-labeled BevF(ab')<sub>2</sub>, the F(ab')<sub>2</sub> fragment of the anti-VEGF antibody bevacizumab can detect the in vivo VEGF changes induced by small molecule tyrosine kinase inhibitors noninvasively and sensitively.<sup>24,25</sup> To investigate whether optical imaging of VEGF expression could be used for the early assessment of tumor responses to cetuximab immunotherapy, in this study we prepared an optical imaging probe by conjugating ranibizumab (Lucentis), a recombinant VEGF-specific mAb Fab fragment, with a NIRF dye.

Longitudinal optical imaging was then performed in both KRAS wild-type HT-29<sup>26</sup> and KRAS mutant HCT-116<sup>27</sup> colon cancer mouse models.

## EXPERIMENTAL SECTION

**Cell Culture and Animal Models.** HT-29 and HCT-116 human colon cancer cell lines were obtained from American Type Culture Collection (ATCC). Cells were grown in culture medium supplemented with 10% fetal bovine serum (FBS) at 37 °C in humidified atmosphere containing 5% CO<sub>2</sub>. All animal experiments were performed in accordance with the Guidelines of Peking University Health Science Center Animal Care and Use Committee. To establish the HT-29 and HCT-116 subcutaneous tumor models, 5 × 10<sup>6</sup> tumor cells were inoculated subcutaneously into the right front flanks of female BALB/c nude mice. The tumor growth was measured using a caliper, and the tumor volume was calculated using the formula volume = length × width<sup>2</sup>/2.

**Competition Binding Assay.** The immunoreactivities of ranibizumab and bevacizumab to human VEGF (hVEGF) or mouse VEGF (mVEGF) were compared by a competition binding assay using <sup>125</sup>I-ranibizumab as the VEGF-specific radioligand. <sup>125</sup>I-ranibizumab was prepared by radiolabeling ranibizumab with Na<sup>125</sup>I using a previously described method.<sup>28</sup> Experiments were performed in VEGF-coated 96-well plates. These plates were prepared by incubating recombinant human VEGF121 (5 µg/mL in bicarbonate buffer, pH = 9.0) or recombinant mouse VEGF120 (5 µg/mL in bicarbonate buffer, pH = 9.0) overnight at 4 °C in high-binding 96-well Stripwell enzyme-linked immunosorbent assay (ELISA) plates (100 µL per well). <sup>125</sup>I-ranibizumab (5.55 kBq) was added to the plates in the presence of increased concentrations of ranibizumab or bevacizumab. After 2 h of reaction at room temperature, the plates were washed with phosphate-buffered saline (PBS). Each well was rinsed, collected in a tube, and then measured in a γ-counter. The best-fit 50% inhibitory concentration (IC<sub>50</sub>) values were calculated by fitting the data through nonlinear regression using Graph Pad Prism 4.0 (GraphPad Software, Inc.). Experiments were performed twice using quadruple samples.

**ELISA.** The hVEGF secreted by HT-29 and HCT-116 tumor cells was determined by ELISA using a previously described method.<sup>24</sup> Briefly, the supernatants of tumor cells grown in 24-well plates were collected and the VEGF levels were determined using a hVEGF ELISA kit and mVEGF (as a negative control) ELISA kit, respectively. Tumor cells in the plates were trypsinized, stained with trypan blue, and counted. The ELISA values were normalized to the number of live cells.

To measure the levels of circulating hVEGF released from the tumor xenografts, five HT-29 tumor-bearing nude mice (tumor size: ~200 cm<sup>3</sup>) were sacrificed. The hVEGF levels in the serum and tumor lysates were determined by an ELISA kit and normalized to the protein concentration measured using the microbicinchoninic acid protein assay kit.

**Near-Infrared Imaging Probe.** Ranibizumab was conjugated with a DyLight755-NHS ester (Pierce, Rockford, IL) according to a standard protocol. Typically, DyLight755-NHS (10 mg/mL) was mixed with ranibizumab in the bicarbonate buffer (pH = 9.0) at a molar ratio of 8:1. After incubation at room temperature for 1 h, the DyLight755-ranibizumab conjugate (denoted as Dye755-Ran) was purified by PD-10 desalting column (GE Healthcare, Piscataway, NJ). The degree of labeling (dye/protein ratio) for Dye755-Ran was calculated

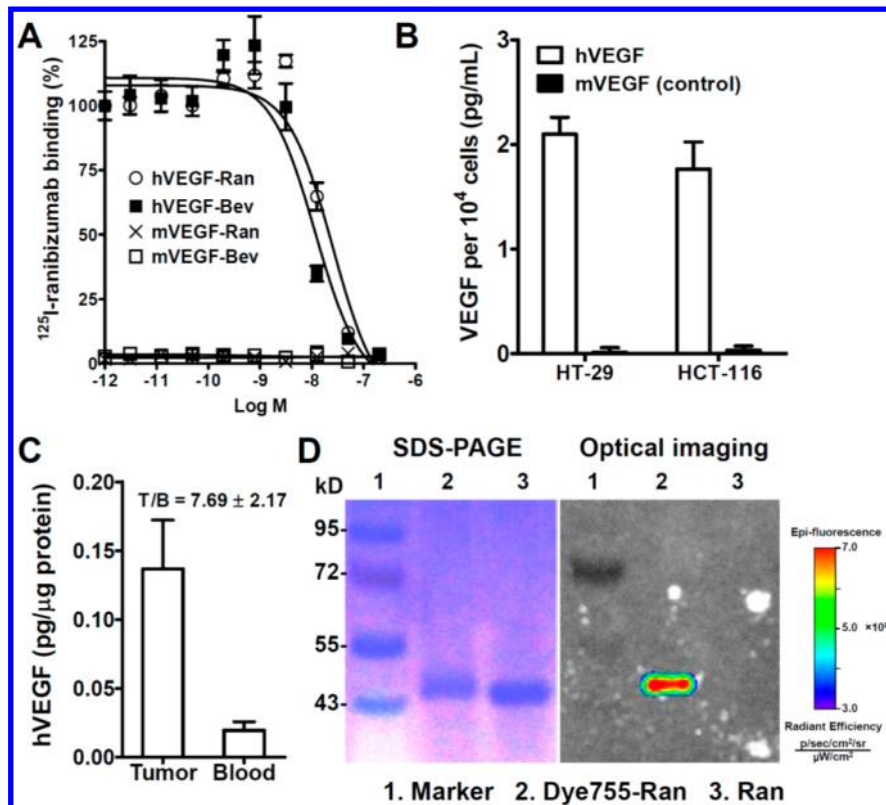


**Figure 1.** (A) Inhibition of  $^{125}\text{I}$ -ranibizumab binding to human VEGF (hVEGF) or mouse VEGF (mVEGF)-coated ELISA plates by ranibizumab (Ran) and bevacizumab (Bev). (B) Quantification of hVEGF levels in cell culture supernatants of HT-29 and HCT-116 cells. Mouse VEGF levels were also determined as negative controls. (C) Human VEGF expression levels in the tumor lysates and serum of HT-29 tumor-bearing nude mice as determined by ELISA. (D) SDS-PAGE and optical imaging of Dye755-Ran and Ran.

to be 4.3 based on UV measurements of  $A_{280}$  and  $A_{755}$ . The purity of Dye755-Ran was characterized by sodium dodecyl sulfate-polyacrylamide gel electrophoresis (SDS-PAGE) and subsequent optical imaging using a small-animal *in vivo* imaging system (IVIS, excitation = 745 nm, emission = 800 nm).

**Cetuximab Therapeutic Efficacy.** The therapeutic efficacy of cetuximab was tested in both HT-29 and HCT-116 tumor-bearing nude mouse models. The animals were segregated into two groups and then intraperitoneally (i.p.) administered with phosphate-buffered saline (PBS) or five doses of cetuximab (200  $\mu\text{g}$  daily for 5 days;  $n = 12$  per group). The tumor size and body weight were measured every other day. On day 5, five animals from each group were sacrificed, and the tumor samples were collected. Half of each tumor sample was immediately frozen in optimal cutting temperature medium (Sakura Finetek USA, Inc.), and then cut into 5  $\mu\text{m}$  thick slices for immunofluorescence staining. The other half of each tumor was homogenized and lysed. The protein concentration and the hVEGF levels were then measured with ELISA kits as previously described.<sup>24</sup>

**Immunofluorescence Staining.** CD31 and Ki67 fluorescence staining studies were performed to determine the effect of cetuximab on tumor vasculature and cell proliferation. After blocking with 10% FBS (in PBS) for 30 min, the frozen tumor slices were incubated with rat antimouse CD31 (1:100; BD Biosciences, San Jose, CA) and rabbit anti-Ki67 (1:100; Chemicon, Millipore, Billerica, MA) antibodies for 1 h at room temperature and then visualized with dye-conjugated secondary antibodies under a Leica TCS-NT confocal microscope (Wetzler, Heidelberg, Germany). After staining, microvascular

density (MVD) values were determined by counting and averaging the number of CD31-positive vessels with 20 fields of view. The tumor proliferation index was calculated using the percentage of Ki67-positive cells in 20 fields of view.

**In Vivo Fluorescence Imaging.** Serial optical imaging (days 0, 3, and 5) of tumor response to cetuximab therapy was performed in both HT-29 and HCT-116 tumor models. For each scan, the mice were i.v. injected with 0.5 nmol of Dye755-Ran, and *in vivo* optical imaging was performed at 2 h p.i. After the baseline scanning (day 0), cetuximab (200  $\mu\text{g}$ ) was i.p. administered once daily for 5 days in the treatment groups. PBS was used in the control groups ( $n = 5$  per group). Optical imaging was repeated on days 3 and 5 under the same conditions. For each scan, an aliquot with 1/20 of the total injection dose was simultaneously subjected to optical imaging. Identical illumination settings were used to obtain all scans. The quantification of Dye755-Ran was performed using a previously described method.<sup>24,25,29–31</sup> Briefly, the region-of-interest (ROI) was drawn for each tumor using Living Image software (Xenogen, Alameda, CA). The fluorescence intensity was presented as the average radiant efficiency in the unit of [ $\text{p/sec}/\text{cm}^2/\text{sr}$ ]/[ $\mu\text{W}/\text{cm}^2$ ]. The tumor uptake was calculated by normalizing the tumor fluorescence intensity by the total injection dose.

**Radiolabeling and Biodistribution.** Ranibizumab was radiolabeled with  $\text{Na}^{125}\text{I}$  (PerkinElmer, Waltham, MA) using the Iodogen method as previously described.<sup>28</sup> After purification with a PD-10 column, the radiochemical purity of the final product  $^{125}\text{I}$ -ranibizumab was >97%. HT-29 and HCT-116 tumor-bearing nude mice were i.p. administered with PBS

or cetuximab (200  $\mu$ g daily for 5 days) ( $n = 5$  per group). After treatment, each mouse was injected with 370 kBq of  $^{125}\text{I}$ -ranibizumab via the tail vein. At 2 h p.i., the mice were sacrificed, and tissues and organs were harvested, weighed, and counted in a  $\gamma$ -counter (Packard, Meriden, CT). The results are presented as percentage of injected dose per gram of tissue (% ID/g).

**Statistical Analysis.** Quantitative data are expressed as means  $\pm$  SD. Means were compared using Student's *t* test. *P* values  $<0.05$  were considered statistically significant.

## RESULTS

**Human VEGF-Specificity of Ranibizumab.** We performed competition binding assay to determine the VEGF-specificity of ranibizumab. By comparing with bevacizumab, we observed that the hVEGF-binding affinity of ranibizumab has the same magnitude as bevacizumab ( $25.34 \pm 0.99$  nM vs  $11.62 \pm 1.05$  nM). However, ranibizumab did not bind to mVEGF, demonstrating its hVEGF-specificity (Figure 1A).

**VEGF Expression Patterns in Tumor Cells and Tissues.** To investigate the VEGF expression patterns in tumor cells and tissues, we performed both fluorescence-activated cell sorting (FACS) analysis and ELISA. VEGF was not expressed on the surface of HT-29 and HCT-116 tumor cells (Figure S1A,B, Supporting Information) but was secreted to the cell culture supernatants by the tumor cells (Figure 1B). The supernatants of the cultured cells can significantly block the binding of  $^{125}\text{I}$ -ranibizumab to hVEGF (Figure S1C, Supporting Information), further confirming that both HT-29 and HCT-116 conditioned medium contained tumor cell-secreted hVEGF.

In the HT-29 tumor xenograft model, the hVEGF levels in the tumor lysates and serum were determined by ELISA. As shown in Figure 1C, the hVEGF was  $0.14 \pm 0.03$  and  $0.02 \pm 0.01$  pg/ $\mu$ g protein for the tumor lysates and serum, respectively. Assuming that the total blood volume of a nude mouse (body weight:  $\sim 20$  g) is 2 mL, we can calculate the fraction of circulating hVEGF released from the tumor to be less than 10% (Figure S1D, Supporting Information). These results demonstrated that a very low level of tumor hVEGF was released to the bloodstream.

**In Vivo Therapeutic Efficacy of Cetuximab.** We investigated the therapeutic efficacy of cetuximab in both HT-29 and HCT-116 tumor models. Female nude mice bearing tumor xenografts were treated daily with cetuximab for 5 days. As shown in Figure 2A, cetuximab treatment inhibited HT-29 tumor growth beginning on day 4, and a statistical difference from the control group was observed from day 10 (*P*

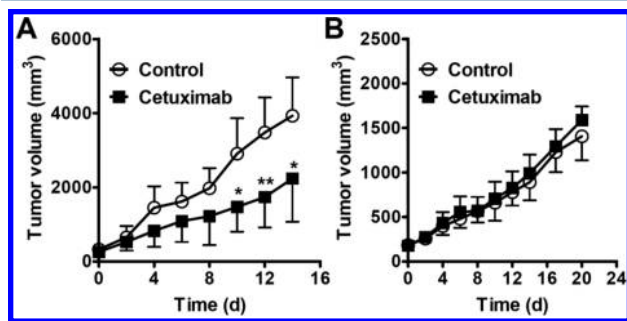


**Figure 2.** In vivo therapeutic efficacy of cetuximab in the KRAS wild-type HT-29 (A) and KRAS mutant HCT-116 (B) tumor models. \*, *P*  $< 0.05$ ; \*\*, *P*  $< 0.01$ .

$< 0.05$ ). Five doses of cetuximab treatment eventually resulted in partial tumor regression in the HT-29 mouse model. In contrast to the antitumor effect of cetuximab in the HT-29 mice, the tumor growth inhibition effect of cetuximab was negligible in the HCT-116 tumor xenografts (Figure 2B).

### Longitudinal NIRF Imaging of VEGF Expression Using Dye755-Ran.

We prepared the VEGF-targeting probe Dye755-Ran by conjugating ranibizumab with a NIRF dye. By SDS-PAGE and the subsequent optical imaging, we confirmed the successful preparation of this probe (Figure 1D). The NIRF imaging results in both HT-29 and HCT-116 tumor-bearing nude mice confirmed the specific VEGF targeting of Dye755-Ran *in vivo* (Figure S2 and S3, Supporting Information). We then performed longitudinal optical imaging studies (on days 0, 3, and 5) with Dye755-Ran to determine the changes in VEGF expression during cetuximab treatment in both HT-29 and HCT-116 tumor-bearing mice. Compared with the control group, the cetuximab-treated HT-29 tumors showed decreased signals of Dye755-Ran on days 3 and 5 (Figure 3A). The quantified percentage fluorescence intensity of Dye755-Ran in the HT-29 tumors is shown in Figure 3B. The uptake values of Dye755-Ran in the cetuximab-treated tumors were significantly lower than that in the control tumors on day 3 ( $3.55 \pm 0.47$  vs  $4.99 \pm 0.76\%$ , *P*  $< 0.01$ ) and day 5

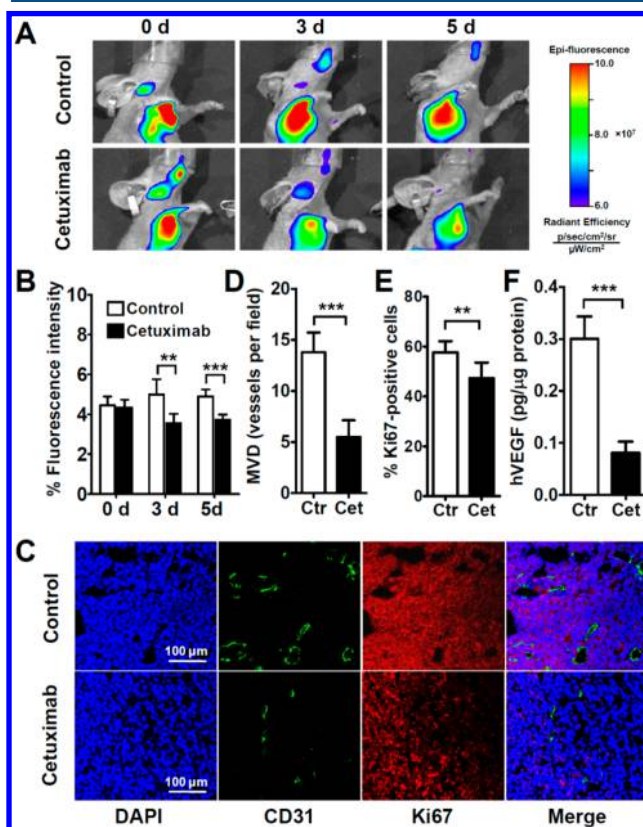


**Figure 3.** (A) Serial *in vivo* optical imaging of HT-29 tumor-bearing nude mice at 2 h after Dye755-Ran injection on days 0, 3, and 5 after cetuximab or PBS treatment. (B) The quantified tumor uptake from panel A. (C) Immunofluorescence staining of CD31 and Ki67 in HT-29 tumor tissues with or without cetuximab treatment. (D–F) Quantified microvascular density (MVD) (D), quantified percentage of Ki67-positive cells (E), and ELISA-determined human VEGF levels (F) in HT-29 tumor tissues with or without cetuximab treatment. \*\*, *P*  $< 0.01$ ; \*\*\*, *P*  $< 0.001$ .

$(3.73 \pm 0.26$  vs  $4.90 \pm 0.34\%$ ,  $P < 0.001$ ). In contrast to the results in the HT-29 tumor model, the fluorescence intensity of Dye755-Ran in the cetuximab-treated HCT-116 tumors was comparable with that in the control tumors (Figure 4A). No significant change in the quantified tumor uptake of Dye755-Ran was observed in the treatment group compared with the control group (Figure 4B).

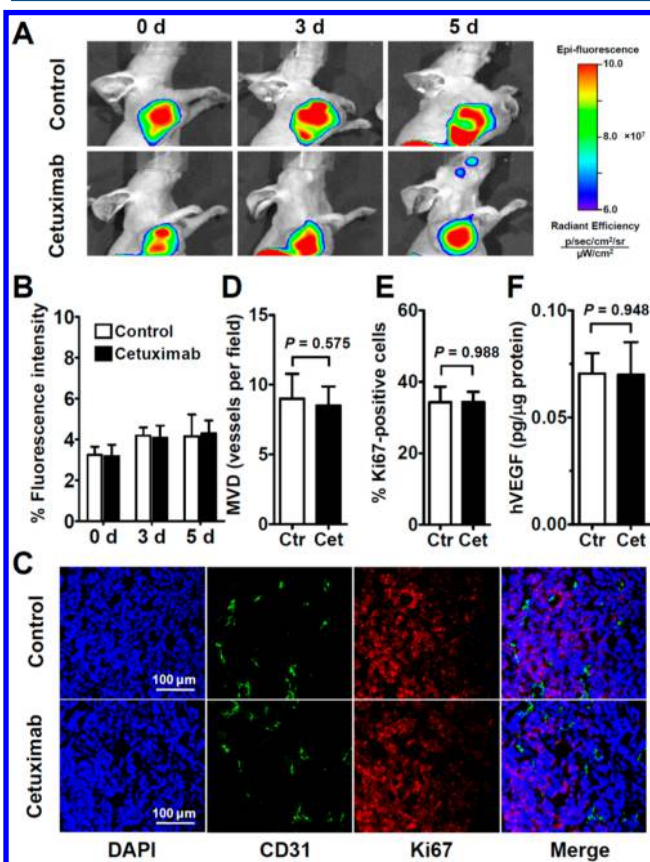


**Figure 4.** (A) Serial in vivo optical imaging of HCT-116 tumor-bearing nude mice at 2 h after Dye755-Ran injection on days 0, 3, and 5 after cetuximab or PBS treatment. (B) The quantified tumor uptake from panel A. (C) Immunofluorescence staining of CD31 and Ki67 in HCT-116 tumor tissues with or without cetuximab treatment. (D–F) Quantified microvascular density (MVD) (D), quantified percentage of Ki67-positive cells (E), and ELISA-determined human VEGF levels (F) in HCT-116 tumor tissues with or without cetuximab treatment.

We performed CD31 and Ki67 immunofluorescence staining to examine the levels of tumor vasculature and cell proliferation in the tumors receiving cetuximab treatment. In the HT-29 tumor model, the cetuximab-treated tumor showed significantly decreased microvascular density ( $13.80 \pm 1.92$  vs  $5.5 \pm 1.64$  vessels per field,  $P < 0.001$ ; Figure 3C,D) and cell proliferation index ( $57.62 \pm 4.51$  vs  $47.27 \pm 6.32\%$ ,  $P < 0.01$ ; Figure 3C,E). In contrast, the microvascular density ( $9.00 \pm 1.79$  vs  $8.50 \pm 1.38$  vessels per field,  $P = 0.575$ ) and cell proliferation index ( $34.27 \pm 4.35$  vs  $34.31 \pm 2.86\%$ ,  $P = 0.988$ ) in the cetuximab-treated tumor were comparable with those of the untreated tumor in the HCT-116 mouse model (Figure 4C–E). The results demonstrated that the treatment efficacy of cetuximab was, at least partially, caused by the inhibition of tumor angiogenesis and tumor cell proliferation.

We performed ELISA to confirm the optical imaging observations on the changes in tumor hVEGF. As shown in Figure 3F, the hVEGF levels in the cetuximab-treated HT-29 tumors were significantly decreased ( $0.08 \pm 0.02$  vs  $0.30 \pm 0.10$  pg/ $\mu$ g protein,  $P < 0.001$ ) compared with those in the control tumors. However, no significant change in hVEGF levels was observed in the cetuximab-treated HCT-116 tumors compared with the control tumors (Figure 4F). Thus, ELISA results confirmed the in vivo Dye755-Ran optical imaging observations on the changes in tumor hVEGF.

**Biodistribution of  $^{125}\text{I}$ -Ranibizumab.** Radioisotope is highly sensitive, and the in vivo behavior of a radiolabeled agent can be accurately quantified by ex vivo biodistribution. Thus, we further validated the optical imaging results of Dye755-ranibizumab by analyzing the biodistribution of  $^{125}\text{I}$ -ranibizumab. The tumor-bearing nude mice were treated with cetuximab or PBS for 5 days. As shown in Figure 5,  $^{125}\text{I}$ -ranibizumab exhibited the highest uptake in the kidney, most likely due to the renal clearance of this radiotracer. The HT-29 tumor uptake of  $^{125}\text{I}$ -ranibizumab in the cetuximab treatment group was significantly lower than that in the control group ( $2.36 \pm 0.23$  vs  $3.40 \pm 0.30\%$  ID/g,  $P < 0.001$ ; Figure 5A). The HCT-116 tumor uptake of  $^{125}\text{I}$ -ranibizumab was  $3.09 \pm 0.88$  and  $3.30 \pm 0.71\%$  ID/g in the cetuximab treatment and control group, respectively ( $P = 0.667$ ; Figure 5B).

## DISCUSSION

We have shown in this study that the antitumor effect of cetuximab can be noninvasively monitored in vivo by optical imaging using a near-infrared dye-labeled ranibizumab (Dye755-Ran). During the cetuximab treatment, the tumor

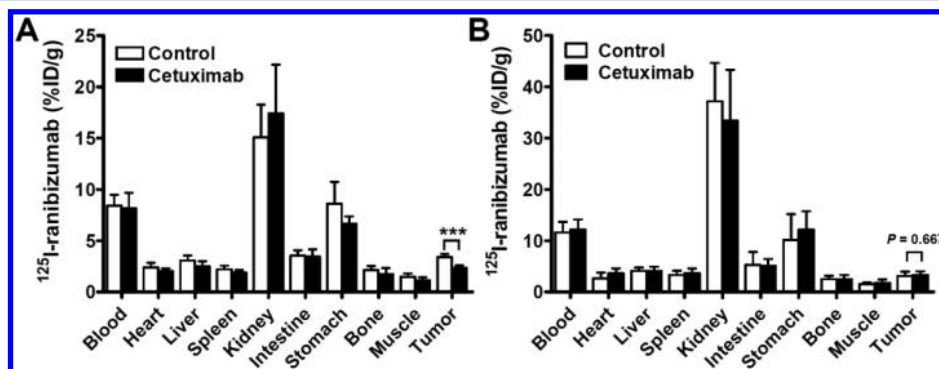


**Figure 5.** Biodistribution of  $^{125}\text{I}$ -ranibizumab in the PBS and cetuximab-treated HT-29 (A) and HCT-116 (B) tumor-bearing nude mice. \*\*\*,  $P < 0.001$ .

uptake of Dye755-Ran was significantly decreased in the responsive HT-29 model, whereas no change in Dye755-Ran uptake was observed in the nonresponsive HCT-116 model. These findings suggested that VEGF expression detected by optical imaging can serve as a biomarker for early tumor response to cetuximab therapy.

*KRAS* gene mutations have been observed in approximately 30% to 50% of mCRC and are common in many other cancers.<sup>32</sup> The presence of mutant *KRAS* in cancers is associated with poor prognosis and with the lack of response to EGFR inhibitor, including cetuximab.<sup>8,10</sup> The antitumor effect of cetuximab was determined in two colon cancer models with different *KRAS* patterns. The *KRAS* gene wild-type HT-29 tumor was responsive to cetuximab, whereas the *KRAS* mutant HCT-116 tumor was not responsive to cetuximab therapy (Figure 2). Cetuximab inhibited tumor growth partly by suppressing tumor cell proliferation as confirmed by reduced Ki67 expression and by inhibiting tumor angiogenesis as confirmed by decreased MVD and VEGF levels.

VEGF is a critical component in tumor proliferation, invasion, and metastasis; several antitumor drugs function by direct or indirect inhibition of the VEGF signaling. Bevacizumab (Avastin) is a humanized monoclonal antibody that specifically binds hVEGF and inhibits its activity, leading to the inhibition of tumor angiogenesis and growth. Recently, bevacizumab has been labeled with radioisotopes and fluorophores for VEGF-targeted tumor imaging<sup>31,33–37</sup> and monitoring of drug-reduced VEGF changes.<sup>38–41</sup> One of the major limitations of molecular imaging using intact antibodies (e.g., bevacizumab) is their prolonged persistence in circulation and nonspecific tumor accumulation because of the enhanced permeability and retention (EPR) effect.<sup>42</sup> Compared with bevacizumab, ranibizumab retains the VEGF-binding domain, but the molecular weight is reduced, which is expected to accelerate blood clearance and subsequently increase the tumor-to-normal tissue contrast.

The high VEGF-binding affinity of ranibizumab was well validated by *in vivo* optical imaging studies in both HCT-116 and HT-29 tumor models. Dye755-Ran showed a similar tumor-targeting property in the two tumor models, and a high tumor uptake was observed as early as 2 h p.i. (Figure S2 and S3, Supporting Information). Since the tumor uptake of macromolecules like ranibizumab at the late time points attributed much to the nonspecific accumulation (e.g., EPR effect),<sup>43</sup> the subsequent longitudinal optical imaging experiments were performed at 2 h after injection to minimize the nonspecific targeting. It should be noted that the *in vivo* behaviors of Dye755-Ran in the present study may not be a true mimicry of the clinical situation because ranibizumab does not bind murine VEGF that expressed in normal mouse organs.

Our serial optical imaging studies clearly demonstrated that Dye755-Ran can differentiate the cetuximab-responsive and nonresponsive tumors as early as 3 d after therapy, which is 7 d earlier than the observed significant decrease in tumor size (Figures 3A,B and 2). The Dye755-Ran uptake decreases in the cetuximab-treated HT-29 tumors but not in the cetuximab-treated HCT-116 tumors. This change in Dye755-Ran uptake correlated well with the down-regulation of hVEGF expression (Figure 3F) and the inhibition of tumor growth (Figure 2). Ranibizumab was previously radiolabeled with <sup>89</sup>Zr, and PET imaging with the resulting radiotracer <sup>89</sup>Zr-ranibizumab allowed the noninvasive determination of angiogenic changes in the tumors treated with the antiangiogenic drug sunitinib.<sup>44</sup> PET

imaging is highly sensitive and can quantitatively determine the expression levels of a tumor target. However, PET radiotracers for longitudinal PET imaging during cancer treatment must be freshly synthesized before each scanning because of their short half-life. The synthesis of PET radiotracers is usually complex and requires postlabeling purification. Meanwhile, different batches of radiotracers have different specific activities, which might result in different *in vivo* biodistributions. Compared with PET radiotracers, an optical imaging probe (e.g., Dye755-Ran) is relatively low cost. The synthesis of an optical imaging probe is also straightforward. The optical imaging probe does not decay and thus can be stored for long-term use. In addition, optical imaging is polychromatic and allows multicolor imaging, which may have broad applications for noninvasive determination of the *in vivo* interactions in living subjects.

In cancer treatment monitoring, optical imaging has two major disadvantages compared with PET- or SPECT-based nuclear imaging methods. First, optical signals have limited tissue penetration depth. NIRF imaging allows efficient photon tissue penetration with minimal intratissue light scattering. However, optical imaging is still inherently limited in terms of detecting relatively superficial tumors, such as breast cancer, thyroid gland tumor, and skin carcinoma. Recent advances in optical imaging techniques can adapt optical imaging for endoscopic use or image-guided surgery,<sup>45</sup> which provides optical imaging access to deep tissues inside the body. The second disadvantage of optical imaging, particularly planar imaging, is its limitation in image reconstruction and quantification. We used a well-validated method<sup>29,31</sup> to quantify the fluorescence intensity, but the quantification may still not be a true reflection of the probe distribution because the images were planar and the fluorescence signal was heterogeneously distributed throughout the tumor tissues. We performed ELISA studies to validate the *in vivo* results of optical imaging. Cetuximab treatment inhibited hVEGF expression in the *KRAS* wild-type HT-29 tumor but not in the *KRAS* mutant HCT-116 tumor. We radiolabeled ranibizumab with <sup>125</sup>I and performed a biodistribution study to further confirm the quantification results of optical imaging. The results clearly confirmed that ranibizumab-based probes can specifically measure the hVEGF changes *in vivo*.

Unlike tumor biomarkers (e.g., EGFR) that are uniquely expressed or markedly overexpressed on tumor cells, VEGF is almost undetectable on the HT-29 and HCT-116 cell surface (Figure S1A and S1B, Supporting Information). Instead, VEGF can be secreted by the tumor cells into cell culture supernatant *in vitro* or be released to the bloodstream *in vivo*. Measurement of the circulating VEGF released from the tumor has been routinely used in the clinical practice for tumor response prediction and monitoring.<sup>46,47</sup> However, circulating biomarkers (e.g., VEGF) have several limitations, the prominent of which is the high frequency of false-positive indications due to the production from normal host tissues.<sup>48</sup> By using ELISA, we observed that in the HT-29 tumor xenografts model, the circulating hVEGF released from the tumor was less than 10%, and more than 90% of the hVEGF was retained in the tumor (Figure S1D, Supporting Information). These results highlighted that quantitative imaging using a probe (e.g., Dye755-Ran) capable of targeting hVEGF at its tissue of origin (i.e., tumor) could be more accurate for determining the hVEGF levels than serum measurements. As in the tumor tissue, VEGF is localized in the extracellular matrix near the tumor vasculature but not on the tumor cell surface, VEGF-targeting

probes (e.g., Dye755-Ran) in the circulation could easily reach the target (Figure S4, Supporting Information), facilitating rapid and specific tumor imaging.

## CONCLUSIONS

We successfully developed a VEGF-specific optical imaging probe Dye755-Ran and demonstrated that Dye755-Ran optical imaging can noninvasively monitor tumor VEGF levels under cetuximab treatment. This strategy can potentially serve as a powerful tool for the early assessment of tumor response to drugs that directly or indirectly act on VEGF, for studying the antiangiogenic mechanisms, and for designing appropriate intervention strategies for tumor angiogenesis.

## ASSOCIATED CONTENT

### Supporting Information

Additional information and methods; FACS analysis of HT-29 and HCT-116 cells;  $^{125}\text{I}$ -ranibizumab binding assay; calculated hVEGF distribution in the HT-29 tumor xenografts model; representative optical images and the quantified tumor uptake of Dye755-Ran in HT-29 and HCT-116 tumor-bearing mice; schematic diagram of in vivo Dye755-Ran tumor targeting. This material is available free of charge via the Internet at <http://pubs.acs.org>.

## AUTHOR INFORMATION

### Corresponding Authors

\*Medical Isotopes Research Center, Peking University, 38 Xueyuan Road, Beijing 100191, China. Tel/Fax: +86-10-82802871. E-mail: liuzf@bjmu.edu.cn.

\*Medical Isotopes Research Center, Peking University, 38 Xueyuan Road, Beijing 100191, China. Tel/Fax: +86-10-82801145. E-mail: wangfan@bjmu.edu.cn.

### Author Contributions

<sup>†</sup>T.M and H.L. contributed equally to this work.

### Notes

The authors declare no competing financial interest.

## ACKNOWLEDGMENTS

This work was supported, in part, by "973" projects (2013CB733802 and 2011CB707705), the NSFC projects (81222019, 81125011, 81371614, 81471712, and 81201127), grants from the Ministry of Science and Technology of China (2011YQ030114, 2012ZX09102301, and 2012BAK25B03), grants from the Ministry of Education of China (31300 and BMU20110263), grants from the Beijing Natural Science Foundation (7132131 and 7132123), and a grant from the Beijing Nova Program (Z121107002512010).

## REFERENCES

- (1) Mendelsohn, J.; Baselga, J. The EGF receptor family as targets for cancer therapy. *Oncogene* **2000**, *19* (56), 6550–65.
- (2) Arteaga, C. L. EGF receptor as a therapeutic target: patient selection and mechanisms of resistance to receptor-targeted drugs. *J. Clin. Oncol.* **2003**, *21* (23 Suppl), 289s–291s.
- (3) Wheeler, D. L.; Dunn, E. F.; Harari, P. M. Understanding resistance to EGFR inhibitors—impact on future treatment strategies. *Nat. Rev. Clin. Oncol.* **2010**, *7* (9), 493–507.
- (4) Chung, K. Y.; Shia, J.; Kemeny, N. E.; Shah, M.; Schwartz, G. K.; Tse, A.; Hamilton, A.; Pan, D.; Schrag, D.; Schwartz, L.; Klimstra, D. S.; Fridman, D.; Kelsen, D. P.; Saltz, L. B. Cetuximab shows activity in colorectal cancer patients with tumors that do not express the epidermal growth factor receptor by immunohistochemistry. *J. Clin. Oncol.* **2005**, *23* (9), 1803–10.
- (5) Wild, R.; Fager, K.; Flefleh, C.; Kan, D.; Inigo, I.; Castaneda, S.; Luo, F. R.; Camuso, A.; McGlinchey, K.; Rose, W. C. Cetuximab preclinical antitumor activity (monotherapy and combination based) is not predicted by relative total or activated epidermal growth factor receptor tumor expression levels. *Mol. Cancer Ther.* **2006**, *5* (1), 104–13.
- (6) Cunningham, D.; Humblet, Y.; Siena, S.; Khayat, D.; Bleiberg, H.; Santoro, A.; Bets, D.; Mueser, M.; Harstrick, A.; Verslype, C.; Chau, I.; Van Cutsem, E. Cetuximab monotherapy and cetuximab plus irinotecan in irinotecan-refractory metastatic colorectal cancer. *N. Engl. J. Med.* **2004**, *351* (4), 337–45.
- (7) Saltz, L. B.; Meropol, N. J.; Loehrer, P. J., Sr.; Needle, M. N.; Kopit, J.; Mayer, R. J. Phase II trial of cetuximab in patients with refractory colorectal cancer that expresses the epidermal growth factor receptor. *J. Clin. Oncol.* **2004**, *22* (7), 1201–8.
- (8) Normanno, N.; Tejpar, S.; Morgillo, F.; De Luca, A.; Van Cutsem, E.; Ciardiello, F. Implications for KRAS status and EGFR-targeted therapies in metastatic CRC. *Nat. Rev. Clin. Oncol.* **2009**, *6* (9), 519–27.
- (9) Allegra, C. J.; Jessup, J. M.; Somerfield, M. R.; Hamilton, S. R.; Hammond, E. H.; Hayes, D. F.; McAllister, P. K.; Morton, R. F.; Schilsky, R. L. American Society of Clinical Oncology provisional clinical opinion: testing for KRAS gene mutations in patients with metastatic colorectal carcinoma to predict response to anti-epidermal growth factor receptor monoclonal antibody therapy. *J. Clin. Oncol.* **2009**, *27* (12), 2091–6.
- (10) Lievre, A.; Bachet, J. B.; Le Corre, D.; Boige, V.; Landi, B.; Emile, J. F.; Cote, J. F.; Tomasic, G.; Penna, C.; Ducreux, M.; Rougier, P.; Penault-Llorca, F.; Laurent-Puig, P. KRAS mutation status is predictive of response to cetuximab therapy in colorectal cancer. *Cancer Res.* **2006**, *66* (8), 3992–5.
- (11) Dolgin, E. FDA narrows drug label usage. *Nature* **2009**, *460* (7259), 1069.
- (12) Khambata-Ford, S.; Garrett, C. R.; Meropol, N. J.; Basik, M.; Harbison, C. T.; Wu, S.; Wong, T. W.; Huang, X.; Takimoto, C. H.; Godwin, A. K.; Tan, B. R.; Krishnamurthi, S. S.; Burris, H. A., 3rd; Poplin, E. A.; Hidalgo, M.; Baselga, J.; Clark, E. A.; Mauro, D. J. Expression of epiregulin and amphiregulin and K-ras mutation status predict disease control in metastatic colorectal cancer patients treated with cetuximab. *J. Clin. Oncol.* **2007**, *25* (22), 3230–7.
- (13) Marusyk, A.; Polyak, K. Tumor heterogeneity: causes and consequences. *Biochim. Biophys. Acta* **2010**, *1805* (1), 105–17.
- (14) Tolmachev, V.; Stone-Elander, S.; Orlova, A. Radiolabelled receptor-tyrosine-kinase targeting drugs for patient stratification and monitoring of therapy response: prospects and pitfalls. *Lancet Oncol.* **2010**, *11* (10), 992–1000.
- (15) Dahabreh, I. J.; Terasawa, T.; Castaldi, P. J.; Trikalinos, T. A. Systematic review: Anti-epidermal growth factor receptor treatment effect modification by KRAS mutations in advanced colorectal cancer. *Ann. Int. Med.* **2011**, *154* (1), 37–49.
- (16) Achmad, A.; Hanaoka, H.; Yoshioka, H.; Yamamoto, S.; Tominaga, H.; Araki, T.; Ohshima, Y.; Oriuchi, N.; Endo, K. Predicting cetuximab accumulation in KRAS wild-type and KRAS mutant colorectal cancer using  $^{64}\text{Cu}$ -labeled cetuximab positron emission tomography. *Cancer Sci.* **2012**, *103* (3), 600–5.
- (17) Barrett, T.; Koyama, Y.; Hama, Y.; Ravizzini, G.; Shin, I. S.; Jang, B. S.; Paik, C. H.; Urano, Y.; Choyke, P. L.; Kobayashi, H. In vivo diagnosis of epidermal growth factor receptor expression using molecular imaging with a cocktail of optically labeled monoclonal antibodies. *Clin. Cancer Res.* **2007**, *13* (22 Pt 1), 6639–48.
- (18) Ferrara, N.; Gerber, H. P.; LeCouter, J. The biology of VEGF and its receptors. *Nat. Med.* **2003**, *9* (6), 669–76.
- (19) Ferrara, N.; Hillan, K. J.; Gerber, H. P.; Novotny, W. Discovery and development of bevacizumab, an anti-VEGF antibody for treating cancer. *Nat. Rev. Drug Discovery* **2004**, *3* (5), 391–400.

- (20) Marshall, J. L. Vascular endothelial growth factor plus epidermal growth factor receptor dual targeted therapy in metastatic colorectal cancer: synergy or antagonism? *J. Oncol.* **2009**, *2009*, 937305.
- (21) Tabernero, J. The role of VEGF and EGFR inhibition: implications for combining anti-VEGF and anti-EGFR agents. *Mol. Cancer Res.* **2007**, *5* (3), 203–20.
- (22) Larsen, A. K.; Ouaret, D.; El Ouadrani, K.; Petitprez, A. Targeting EGFR and VEGF(R) pathway cross-talk in tumor survival and angiogenesis. *Pharmacol. Ther.* **2011**, *131* (1), 80–90.
- (23) Ellis, L. M. Epidermal growth factor receptor in tumor angiogenesis. *Hematol. Oncol. Clin. North Am.* **2004**, *18* (5), 1007–21 viii.
- (24) Liu, Z.; Sun, X.; Liu, H.; Ma, T.; Shi, J.; Jia, B.; Zhao, H.; Wang, F. Early assessment of tumor response to gefitinib treatment by noninvasive optical imaging of tumor vascular endothelial growth factor expression in animal models. *J. Nucl. Med.* **2014**, *55* (5), 818–23.
- (25) Sun, X.; Ma, T.; Liu, H.; Yu, X.; Wu, Y.; Shi, J.; Jia, B.; Zhao, H.; Wang, F.; Liu, Z. Longitudinal monitoring of tumor antiangiogenic therapy with near-infrared fluorophore-labeled agents targeted to integrin alphabeta and vascular endothelial growth factor. *Eur. J. Nucl. Med. Mol. Imaging* **2014**, *41* (7), 1428–39.
- (26) Dieterle, C. P.; Conzelmann, M.; Linnemann, U.; Berger, M. R. Detection of isolated tumor cells by polymerase chain reaction-restriction fragment length polymorphism for K-ras mutations in tissue samples of 199 colorectal cancer patients. *Clin. Cancer Res.* **2004**, *10* (2), 641–50.
- (27) Okada, F.; Rak, J. W.; Croix, B. S.; Lieubeau, B.; Kaya, M.; Roncari, L.; Shirasawa, S.; Sasazuki, T.; Kerbel, R. S. Impact of oncogenes in tumor angiogenesis: mutant K-ras up-regulation of vascular endothelial growth factor/vascular permeability factor is necessary, but not sufficient for tumorigenicity of human colorectal carcinoma cells. *Proc. Natl. Acad. Sci. U.S.A.* **1998**, *95* (7), 3609–14.
- (28) Liu, Z.; Yu, Z.; He, W.; Ma, S.; Sun, L.; Wang, F. In-vitro internalization and in-vivo tumor uptake of anti-EGFR monoclonal antibody LA22 in A549 lung cancer cells and animal model. *Cancer Biother. Radiopharm.* **2009**, *24* (1), 15–24.
- (29) Chen, X.; Conti, P. S.; Moats, R. A. In vivo near-infrared fluorescence imaging of integrin alphavbeta3 in brain tumor xenografts. *Cancer Res.* **2004**, *64* (21), 8009–14.
- (30) van de Ven, S. M.; Elias, S. G.; Chan, C. T.; Miao, Z.; Cheng, Z.; De, A.; Gambhir, S. S. Optical imaging with her2-targeted affibody molecules can monitor hsp90 treatment response in a breast cancer xenograft mouse model. *Clin. Cancer Res.* **2012**, *18* (4), 1073–81.
- (31) Zhang, Y.; Hong, H.; Engle, J. W.; Yang, Y.; Barnhart, T. E.; Cai, W. Positron emission tomography and near-infrared fluorescence imaging of vascular endothelial growth factor with dual-labeled bevacizumab. *Am. J. Nucl. Med. Mol. Imaging* **2012**, *2* (1), 1–13.
- (32) Amado, R. G.; Wolf, M.; Peeters, M.; Van Cutsem, E.; Siena, S.; Freeman, D. J.; Juan, T.; Sikorski, R.; Suggs, S.; Radinsky, R.; Patterson, S. D.; Chang, D. D. Wild-type KRAS is required for panitumumab efficacy in patients with metastatic colorectal cancer. *J. Clin. Oncol.* **2008**, *26* (10), 1626–34.
- (33) Nagengast, W. B.; de Vries, E. G.; Hospers, G. A.; Mulder, N. H.; de Jong, J. R.; Hollema, H.; Brouwers, A. H.; van Dongen, G. A.; Perk, L. R.; Lub-de Hooge, M. N. In vivo VEGF imaging with radiolabeled bevacizumab in a human ovarian tumor xenograft. *J. Nucl. Med.* **2007**, *48* (8), 1313–9.
- (34) Stollman, T. H.; Scheer, M. G.; Leenders, W. P.; Verrijp, K. C.; Soede, A. C.; Oyen, W. J.; Ruers, T. J.; Boerman, O. C. Specific imaging of VEGF-A expression with radiolabeled anti-VEGF monoclonal antibody. *Int. J. Cancer* **2008**, *122* (10), 2310–4.
- (35) Nayak, T. K.; Garmestani, K.; Baidoo, K. E.; Milenic, D. E.; Brechbiel, M. W. PET imaging of tumor angiogenesis in mice with VEGF-A-targeted <sup>86</sup>Y-CHX-A"-DTPA-bevacizumab. *Int. J. Cancer* **2011**, *128* (4), 920–6.
- (36) Gaykema, S. B.; Brouwers, A. H.; Lub-de Hooge, M. N.; Pleijhuis, R. G.; Timmer-Bosscha, H.; Pot, L.; van Dam, G. M.; van der Meulen, S. B.; de Jong, J. R.; Bart, J.; de Vries, J.; Jansen, L.; de Vries, E. G.; Schroder, C. P. <sup>89</sup>Zr-bevacizumab PET imaging in primary breast cancer. *J. Nucl. Med.* **2013**, *54* (7), 1014–8.
- (37) Terwisscha van Scheltinga, A. G.; van Dam, G. M.; Nagengast, W. B.; Ntzachristos, V.; Hollema, H.; Herek, J. L.; Schroder, C. P.; Kosterink, J. G.; Lub-de Hoog, M. N.; de Vries, E. G. Intraoperative near-infrared fluorescence tumor imaging with vascular endothelial growth factor and human epidermal growth factor receptor 2 targeting antibodies. *J. Nucl. Med.* **2011**, *52* (11), 1778–85.
- (38) Nagengast, W. B.; de Korte, M. A.; Oude Munnink, T. H.; Timmer-Bosscha, H.; den Dunnen, W. F.; Hollema, H.; de Jong, J. R.; Jensen, M. R.; Quadt, C.; Garcia-Echeverria, C.; van Dongen, G. A.; Lub-de Hooge, M. N.; Schroder, C. P.; de Vries, E. G. <sup>89</sup>Zr-bevacizumab PET of early antiangiogenic tumor response to treatment with HSP90 inhibitor NVP-AUY922. *J. Nucl. Med.* **2010**, *51* (5), 761–7.
- (39) van der Bilt, A. R.; Terwisscha van Scheltinga, A. G.; Timmer-Bosscha, H.; Schroder, C. P.; Pot, L.; Kosterink, J. G.; van der Zee, A. G.; Lub-de Hooge, M. N.; de Jong, S.; de Vries, E. G.; Reyners, A. K. Measurement of tumor VEGF-A levels with <sup>89</sup>Zr-bevacizumab PET as an early biomarker for the antiangiogenic effect of everolimus treatment in an ovarian cancer xenograft model. *Clin. Cancer Res.* **2012**, *18* (22), 6306–14.
- (40) Chang, S. K.; Rizvi, I.; Solban, N.; Hasan, T. In vivo optical molecular imaging of vascular endothelial growth factor for monitoring cancer treatment. *Clin. Cancer Res.* **2008**, *14* (13), 4146–53.
- (41) Chang, A. J.; Sohn, R.; Lu, Z. H.; Arbeit, J. M.; Lapi, S. E. Detection of rapalog-mediated therapeutic response in renal cancer xenografts using <sup>64</sup>Cu-bevacizumab immunoPET. *PLoS One* **2013**, *8* (3), e58949.
- (42) Maeda, H.; Fang, J.; Inutsuka, T.; Kitamoto, Y. Vascular permeability enhancement in solid tumor: various factors, mechanisms involved and its implications. *Int. Immunopharmacol.* **2003**, *3* (3), 319–28.
- (43) Heneweer, C.; Holland, J. P.; Divilov, V.; Carlin, S.; Lewis, J. S. Magnitude of enhanced permeability and retention effect in tumors with different phenotypes: <sup>89</sup>Zr-albumin as a model system. *J. Nucl. Med.* **2011**, *52* (4), 625–33.
- (44) Nagengast, W. B.; Lub-de Hooge, M. N.; Oosting, S. F.; den Dunnen, W. F.; Warnders, F. J.; Brouwers, A. H.; de Jong, J. R.; Price, P. M.; Hollema, H.; Hospers, G. A.; Elsinga, P. H.; Hesselink, J. W.; Gietema, J. A.; de Vries, E. G. VEGF-PET imaging is a noninvasive biomarker showing differential changes in the tumor during sunitinib treatment. *Cancer Res.* **2011**, *71* (1), 143–53.
- (45) van Dam, G. M.; Themelis, G.; Crane, L. M.; Harlaar, N. J.; Pleijhuis, R. G.; Kelder, W.; Sarantopoulos, A.; de Jong, J. S.; Arts, H. J.; van der Zee, A. G.; Bart, J.; Low, P. S.; Ntzachristos, V. Intraoperative tumor-specific fluorescence imaging in ovarian cancer by folate receptor-alpha targeting: first in-human results. *Nat. Med.* **2011**, *17* (10), 1315–9.
- (46) Hanrahan, E. O.; Ryan, A. J.; Mann, H.; Kennedy, S. J.; Langmuir, P.; Natale, R. B.; Herbst, R. S.; Johnson, B. E.; Heymach, J. V. Baseline vascular endothelial growth factor concentration as a potential predictive marker of benefit from vandetanib in non-small cell lung cancer. *Clin. Cancer Res.* **2009**, *15* (10), 3600–9.
- (47) Haura, E. B.; Tanvetyanon, T.; Chiappori, A.; Williams, C.; Simon, G.; Antonia, S.; Gray, J.; Litschauer, S.; Tetteh, L.; Neuger, A.; Song, L.; Rawal, B.; Schell, M. J.; Bepler, G. Phase I/II study of the Src inhibitor dasatinib in combination with erlotinib in advanced non-small-cell lung cancer. *J. Clin. Oncol.* **2010**, *28* (8), 1387–94.
- (48) Viola-Villegas, N. T.; Rice, S. L.; Carlin, S.; Wu, X.; Evans, M. J.; Sevak, K. K.; Drobjnak, M.; Ragupathi, G.; Sawada, R.; Scholz, W. W.; Livingston, P. O.; Lewis, J. S. Applying PET to broaden the diagnostic utility of the clinically validated CA19.9 serum biomarker for oncology. *J. Nucl. Med.* **2013**, *54* (11), 1876–82.